THE JOURNAL OF PHYSICAL CHEMISTRY A

Article

Cite This: J. Phys. Chem. A 2018, 122, 3170−3176

pubs.acs.org/JPCA

High-Frequency/High-Field Electron Paramagnetic Resonance and Theoretical Studies of Tryptophan-Based Radicals

Ian Davis,[†,‡,¶] Teruaki Koto,[†,¶] James R. Terrell,[‡] Alexander Kozhanov,[§] J. Krzystek,[∥] and Aimin Liu*[,†]

[†]Department of Chemistry, University of Texas, San Antonio, Texas 78249, United States

[‡]Department of Chemistry, Georgia State University, Atlanta, Georgia 30303, United States

[§]Department of Physics and Astronomy, Georgia State University, Atlanta, Georgia 30303, United States

[∥]National High Magnetic Field Laboratory, Florida State University, Tallahassee, Florida 32310, United States

Supporting Information

ABSTRACT: Tryptophan-based free radicals have been implicated in a myriad of catalytic and electron transfer reactions in biology. However, very few of them have been trapped so that biophysical characterizations can be performed in a high-precision context. In this work, tryptophan derivative-based radicals were studied by high-frequency/high-field electron paramagnetic resonance (HFEPR) and quantum chemical calculations. Radicals were generated at liquid nitrogen temperature with a photocatalyst, sacrificial oxidant, and violet laser. The precise *g*-anisotropies of L- and D-tryptophan, 5-hydroxytryptophan, 5-methoxytryptophan, 5-fluorotryptophan, and 7-hydroxytryptophan were measured directly by HFEPR. Quantum chemical calculations were conducted to predict both neutral and cationic radical spectra for comparison with the experimental data. The results indicate that under the experimental conditions, all radicals formed were cationic. Spin densities of the radicals were also calculated. The various line patterns and *g*-anisotropies observed by HFEPR can be understood in terms of spin-density populations and the positioning of oxygen atom substitution on the tryptophan ring. The results are considered in the light of the tryptophan and 7-hydroxytryptophan diradical found in the biosynthesis of the tryptophan tryptophylquinone cofactor of methylamine dehydrogenase.

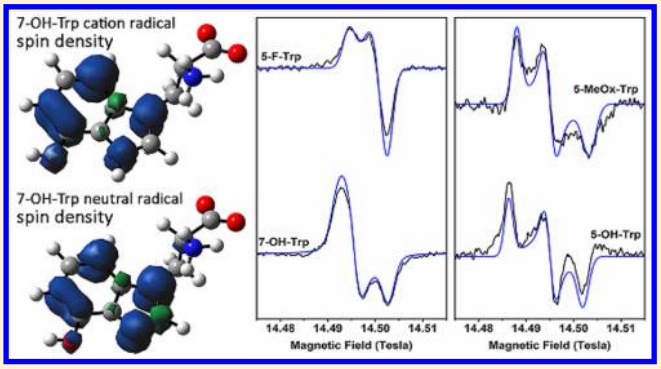

INTRODUCTION

The essential amino acid tryptophan is used both as a building block for proteins and as a precursor of various bioactive compounds. In mammals, tryptophan not utilized for protein synthesis is catabolized by two major pathways: kynurenine and serotonin biosynthesis. In the brain, tryptophan is transformed to serotonin and then melatonin, two molecules involved in mood and sleep, respectively.[1,2] In other tissues, mostly liver, the kynurenine pathway is capable of transforming tryptophan to alanine and acetoacetate via glutaryl−coenzyme A for energy production. The kynurenine pathway also produces several neuroactive side products, one of which is the precursor for nicotinamide adenine dinucleotide biosynthesis.[3−6]

As a protein building block, tryptophan is used for structural roles[7] and electron transport[8,9] and is occasionally modified to serve as a cofactor for various enzymes.[10,11] Tryptophan also plays important redox roles in biology. Tryptophan-based free radicals have been found in cytochrome *c* peroxidase,[12] *Bulkholderia pseudomallei* catalase-peroxidase,[13] lignin peroxidase,[14] versatile peroxidase,[15] and mutagenic or modified forms of azurin and ribonucleotide reductase.[16−19] One notable example of tryptophan being used as radical intermediates for synthesis of an enzyme cofactor is in methylamine dehydrogenase (MADH). The active site of MADH contains a tryptophan tryptophylquinone (TTQ) cofactor consisting of two cross-linked tryptophan residues, one of which has been hydroxylated at the 6 and 7 positions and oxidized to the corresponding quinone.[10] The TTQ cofactor is generated from a precursor protein, preMADH, which contains no cross-link and only one hydroxylation at the 7-position, as shown in Scheme 1, by the diheme enzyme MauG.[20] MauG is able to achieve redox cycle between its resting diferric and a high-valent *bis*-Fe(IV) species, which carries two oxidizing equivalents.[21] The *bis*-Fe(IV) state of MauG has been shown to be able to oxidize preMADH, generating two distinct radicals reported as a tryptophan and a 7-hydroxytryptophan radical that undergo spontaneous radical recombination and deprotonation to form the cross-link necessary for TTQ formation.[22] The two radicals observed in preMADH upon oxidation by *bis*-Fe(IV) MauG display *g*-

Received: December 18, 2017
Revised: February 23, 2018
Published: February 28, 2018

ACS Publications © 2018 American Chemical Society

DOI: 10.1021/acs.jpca.7b12434
J. Phys. Chem. A 2018, 122, 3170−3176

Scheme 1. Crosslink Formation in preMADH during TTQ Biosynthesis and Compounds under Investigation in This Study

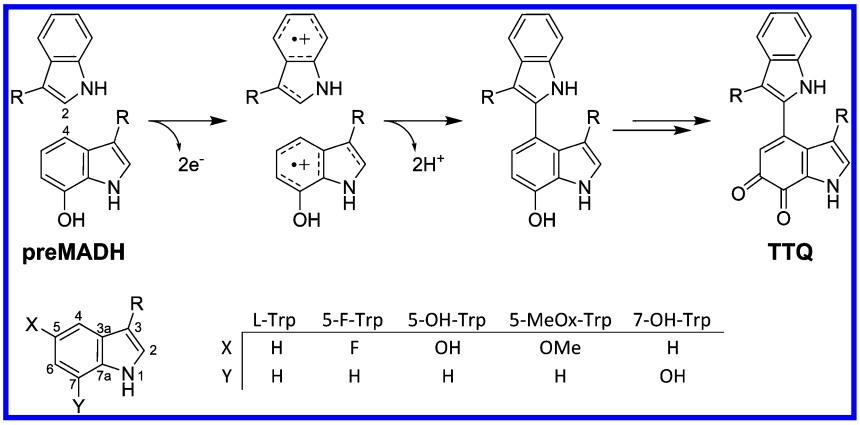

anisotropy intermediate between other measured tryptophan and tyrosine radicals.[23]

In the initial EPR characterization of the intermediate formed upon reaction of preMADH with *bis*-Fe(IV) MauG, stoichiometry and spin quantitation indicated that two radicals were formed on preMADH concomitant with the reduction of MauG to its resting diferric state. EPR spectra of the preMADH-based intermediate measured at X-band (9 GHz) were unable to determine whether the signals arose from multiple similar species or multiple equivalents of a single species. Therefore, high-frequency/high-field (HFEPR) studies with a 15 T magnet were pursued.[22] Measurements of the preMADH-based radical at 416 GHz revealed two sets of overlapping signals with differing *g*-anisotropies. On the basis of the *g*-anisotropies ($\Delta g(g_z - g_x)$), overall reaction, and crystal structure of preMADH and MADH, the two radical species were assigned to the tryptophan and 7-hydroxytryptophan (7-OH-Trp) which are cross-linked during TTQ biosynthesis, with the latter assigned to the signal with larger *g*-value anisotropy.[22]

If the two radicals observed in the preMADH-based intermediate are indeed the residues involved in forming the cross-linked TTQ cofactor, the close proximity of these two residues (ca. 3 Å from edge to edge) raises an immediate question as to why no through-space coupling interactions are observed in the EPR spectra. Two radical species at such a distance would be expected to interact with each other. In the case of weak exchange, an exchange-coupling interaction would be expected to produce a much broader signal. But line broadening was not observed from the preMADH diradical EPR spectrum. Strong interactions such as antiferromagnetic coupling would lead to an EPR silent species, whereas ferromagnetic coupling would produce an integer spin system with resonances appearing in different locations due to zero-field splitting contributions.[24]

One potential explanation for the lack of coupling may be that the close proximity of two cation radicals enforced by the protein scaffold in preMADH may perturb the spin density distributions of the radicals or cause electrostatic repulsion. An additional complication to interpreting the previous findings is that no other 7-OH-Trp radical has been previously characterized by EPR spectroscopy, so it is impossible to know what features observed in the diradical intermediate are intrinsic to the 7-OH-Trp and how those features may be perturbed in the context of a diradical species. The closest example is a UV−vis absorbance study of the 7-hydroxyindole radical.[25] Therefore, there is a need to analyze HFEPR spectra of isolated tryptophan and 7-OH-Trp to provide insight into the contributions made by the close proximity of two cation radicals and the protein scaffold on the radical spectra.

In this work, we adapted a recently developed rhenium/ruthenium-based photocatalyst to generate organic radicals.[26] This novel method has been successfully used in the transient kinetics study of tyrosyl radicals in solution. Here, we extended this approach to spectroscopically characterize tryptophan radicals in solid state at cryogenic temperatures. The resulting tryptophan and various tryptophan derivative-based radicals are amenable to characterization by HFEPR. The results are interpreted with quantum chemical calculations to clarify the effects of substituents on the *g*-anisotropy of tryptophan-based radicals.

MATERIALS AND METHODS

Chemicals. All chemicals including the Ru(III) complex were purchased from Sigma-Aldrich in their highest available purity and were used without further purification with the exception of 7-hydroxytryptophan which was purchased from Ryan Scientific Inc.

Synthesis of Photocatalyst. Tricarbonyl(1,10-phenanthroline)(4-hydroxymethylpyridyl)rhenium(I) hexafluorophosphate, $[Re(phen)(CO)_3(PyCH_2OH)]PF_6$, was prepared by a literature method.[26] Briefly, $[Re(phen)(CO)_3(NCMe)]PF_6$ was dissolved in tetrahydrofuran with $PyCH_2OH$, and the mixture was heated under reflux for 18 h. The product was purified to analytically pure form by recrystallization after exchanging solvent to a minimal amount of DCM and slow addition of diethyl ether.

EPR Spectroscopy. Compounds under study were dissolved in 40% phosphoric acid with the rhenium photocatalyst and ruthenium sacrificial oxidant before being frozen in liquid nitrogen at 1, 1.5, and 5 mM, respectively. Frozen samples were irradiated at 77 K for 30 min with a 405 nm, 120 mW laser. Radical formation was verified by X-band (9 GHz) EPR spectroscopy, and the experimental conditions were optimized on the basis of the X-band EPR results. HFEPR samples were generated in sample cups of ca. 150 μL volume.[22] HFEPR spectra were recorded at the EMR Facility at the National High Magnetic Field Laboratory in Tallahassee, FL. The 15-T magnet-based spectrometer has been described previously.[27] All spectra were acquired at 4.5 K, 406.4 GHz, and 0.3 mT modulation amplitude with the presence of an atomic hydrogen standard to calibrate the magnetic field.[28] A series of experiments was also performed on a 25 T resistive "Keck"

DOI: 10.1021/acs.jpca.7b12434
J. Phys. Chem. A 2018, 122, 3170−3176

magnet in the DC Facility at ~700 GHz.[29] HFEPR simulations of the experimental spectra were performed using the EPR simulation program DOUBLET.[30]

Quantum Chemical Calculations. All calculations were implemented with the ORCA quantum chemistry program package (version 3.0.3).[31] Full geometry optimizations were performed using the B3LYP hybrid functional with RIJCOSX approximation[32,33] in combination with the def2-TZVP(-f) basis set for all atoms with tight SCF convergence criteria for both cation and neutral radical forms of tryptophan and four substituted tryptophan derivatives: 7-hydroxytryptophan (7-OH-Trp), 5-hydroxytryptophan (5-OH-Trp), 5-methoxytryptophan (5-MeOx-Trp), and 5-fluorotryptophan (5-F-Trp). The basis sets used for geometry optimization were also used for *g*-tensor and spin population calculations. The calculations included consideration of solvent effects assuming the presence of a dielectric continuum with the conductor-like screening model (COSMO)[34] and the dielectric constant of water.[35]

RESULTS AND DISCUSSION

Solid-State, Photocatalytic Radical Generation. Tryptophan free radicals are short-lived, with an estimated $t_{1/2}$ of less than 1 ms in solution. To circumvent this issue, we adapted a recently developed photocatalyst method by Nocera et al., which has been used by others to generate tyrosyl radicals in solution for transient absorption spectroscopy,[26] and optimized it for HFEPR studies. As illustrated in Scheme 2, the radical

Scheme 2. Photocatalytic Method for Generating Tryptophan-Based Radicals

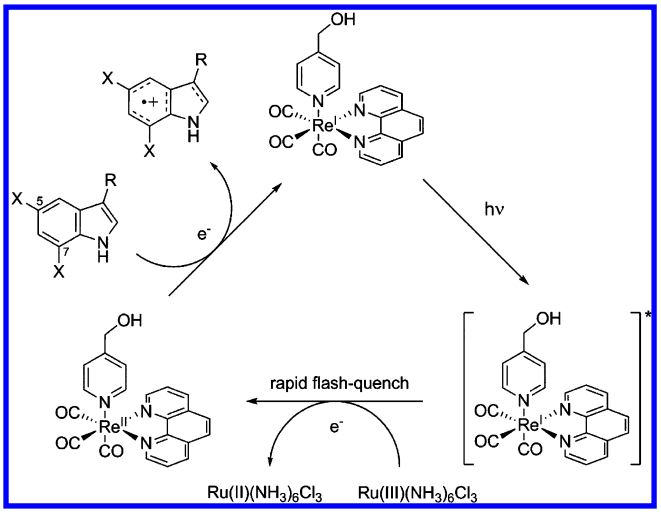

species were generated with the use of a rhenium photocatalyst and ruthenium sacrificial oxidant. All compounds, L-Trp, D-Trp, 5-F-Trp, 5-MeOx-Trp, 5-OH-Trp, and 7-OH-Trp, were dissolved in 40% phosphoric acid, respectively, with photocatalyst and sacrificial oxidant so that the frozen solutions would form a transparent glass, allowing facile photoexcitation of the rhenium catalyst at cryogenic temperatures. Solubility issues arose with other common glass-forming solvents.[36] The oxidation of tryptophan and several of its analogues, including 7-OH-Trp, were initiated by photoexcitation of the rhenium complex. The excited-state rhenium complex is then oxidized by the sacrificial ruthenium oxidant. The oxidized Re(II) species can in turn oxidize tryptophan or one of its analogues to its respective radical, presumably cation, species. Because the radical is formed at cryogenic temperatures, it is not rapidly quenched. Also, the photocatalytic method allows for the use of nonionizing violet light, which prevents the formation of solvated electrons or multiple undesirable radical species that might otherwise interfere with species of interest.

HFEPR Characterization. The radical forms of L-Trp, D-Trp, 5-F-Trp, 5-MeOx-Trp, 5-OH-Trp, and 7-OH-Trp were successfully generated by the photocatalytic method and subsequently analyzed by HFEPR spectroscopy after optimization of the experimental conditions. Exclusion of any of the elements, photocatalyst, sacrificial oxidant, indole derivative, or laser light gave rise to samples with no radical signals. Aside from D- and L-tryptophan, all other compounds studied were racemic mixtures. The presence of concentrated phosphoric acid, catalyst, or sacrificial oxidant resulted in significant absorption of the transmitted sub-THz wave power, which in turn limited the signal-to-noise ratio of the spectra. However, with sufficient averaging, the spectra were fully interpretable. Experiments at higher frequency/field (~700 GHz/25 T, respectively) were, however, unsuccessful. Due to increased power losses through the solvent at elevated sub-THz frequencies, the resulting spectra were not amenable to analysis due to very low S/N ratio, even with averaging.

Figure 1 shows the HFEPR spectra of tryptophan radicals generated by the photocatalytic method. Three distinct spectral patterns can be recognized for the experimental HFEPR spectra: axial with *g*-parallel larger than *g*-perpendicular for Trp and 5-F-Trp; axial with *g*-parallel smaller than *g*-perpendicular

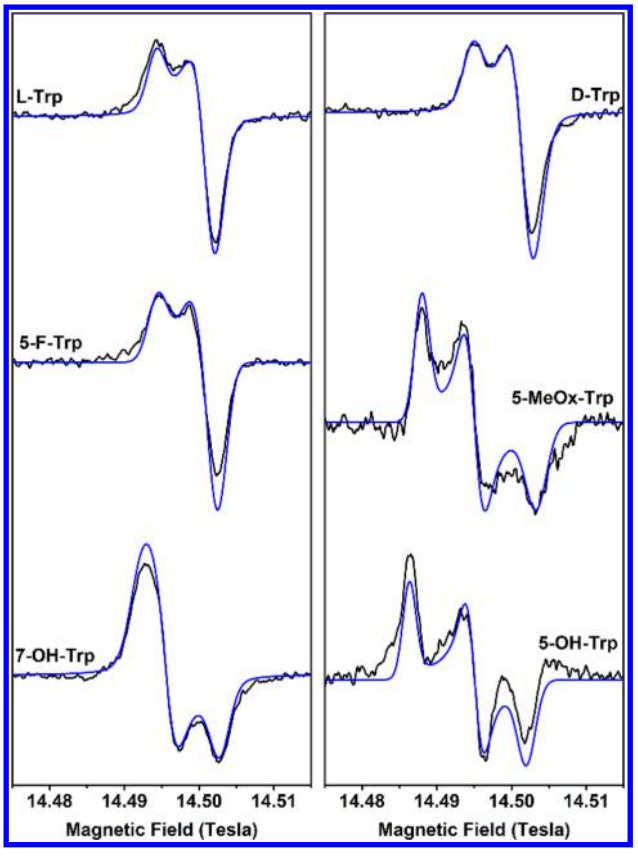

Figure 1. HFEPR spectra of tryptophan-based radicals at 406.4 GHz, 0.3 mT modulation amplitude, 4.5 K (black trace) and corresponding simulated spectra (blue trace). Simulation parameters can be found in Table 1.

DOI: 10.1021/acs.jpca.7b12434
J. Phys. Chem. A 2018, 122, 3170−3176

Table 1. Experimentally Determined and Calculated *g*-Values for Tryptophan Derivatives

		g_{min}	g_{mid}	g_{max}	span[a]	span/L-Trp	skew[b]
L-Trp	experiment	2.00227	2.00240	2.00329	102		0.873
	cation	2.00226	2.00255	2.00325	99		0.698
	neutral	2.00225	2.00288	2.00366	140		0.551
7-OH-Trp	experiment	2.00213	2.00313	2.00358	145	1.422	0.310
	cation	2.00225	2.00318	2.00360	135	1.361	0.312
	neutral	2.00225	2.00303	2.00407	183	1.300	0.574
5-OH-Trp	experiment	2.00223	2.00319	2.00439	216	2.118	0.556
	cation	2.00224	2.00321	2.00427	203	2.043	0.521
	neutral	2.00224	2.00322	2.00416	192	1.368	0.488
5-MeOx-Trp	experiment	2.00205	2.00319	2.00416	211	2.069	0.460
	cation	2.00223	2.00335	2.00442	219	2.213	0.491
	neutral	2.00225	2.00313	2.00451	226	1.608	0.608
5-F-Trp	experiment	2.00217	2.00244	2.00327	110	1.078	0.755
	cation	2.00227	2.00256	2.00322	95	0.959	0.695
	neutral	2.00227	2.00290	2.00375	148	1.052	0.575

[a]Span is Δg, the difference between g_{min} and $g_{max} \times 10^5$. [b]Skew is $g_{max} - g_{mid}/g_{max} - g_{min}$.

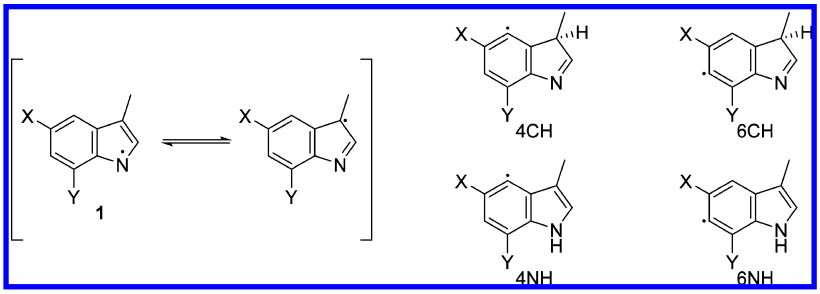

Figure 2. Potential neutral radical structures resulting from π-radical delocalization over the indole ring.

for 7-OH-Trp; and rhombic for 5-OH-Trp and 5-MeOx-Trp. Experimentally determined *g*-values and Δg are summarized in Table 1, and the full spectrum of each radical including the magnetic field standard[28] and simulation can be found in Supplementary Figures S1−S6. X-band EPR spectra of L-Trp, 5-OH-Trp, 5-MeOx-Trp, and 7-OH-Trp can be found in Supplementary Figures S7−S10. Spectra of L- and D-tryptophan both produce axial EPR spectra with slightly different principal *g*-values; however, they have very similar *g*-anisotropies (Δg, $g_{max} - g_{min}$) of 102×10^{-5} and 100×10^{-5}, respectively. Even at the magnetic fields used for this study (15 T), all the principal *g*-values of tryptophan cannot be fully resolved, and the radicals produce axial spectra with g_{min} and g_{mid} largely overlapping. Replacing hydrogen in the 5-position with a highly electronegative fluorine, 5-F-Trp, did not perturb the line shape; however, it did lead to a slight increase in the Δg to 110×10^{-5}.

Substitution at the 5-position with a methoxy or hydroxyl group, 5-MeOx-Trp and 5-OH-Trp, respectively, however, gave rise to rhombic signals with completely resolved *g*-values and a doubling of the Δg to 211×10^{-5} and 216×10^{-5}, respectively. Similarly to the unsubstituted tryptophan, substitution with a hydroxyl group at the 7-position, 7-OH-Trp, gives rise to an axial signal; however, in this case, the g_{mid} and g_{max} could not be resolved, opposite to what was seen with the unsubstituted tryptophan. The 7-OH-Trp radical also showed an increased Δg, intermediate between unsubstituted tryptophan and 5-OH-Trp at 145×10^{-5}. The *g*-anisotropy has been previously found to be a sensitive indicator for differentiating tyrosyl and tryptophanyl radicals.[18,22,37] The OH substitution on the phenyl ring of tryptophan is anticipated to increase the Δg value. Comparing 7-OH-Trp and L-Trp radicals, the ratio of the Δg for the photogenerated species is 1.422, slightly larger than the 1.352 obtained from HFEPR spectra of enzymatically oxidized preMADH.[22]

Quantum Chemical Calculations. Density functional theory calculations were performed to interpret the origin of the above experimental findings theoretically in terms of spin populations and *g*-tensors for both cation and neutral radical forms of the compounds measured. Cationic radical structures are derived from their parent indole derivative less one electron; however, there is some ambiguity as to what chemical structure may be most appropriate for a neutral radical species. Geometry optimization and energy calculation indicate that only structures in which the indole nitrogen is deprotonated should be used for further consideration, as other possible neutral radicals are significantly higher in energy, as shown in Figure 2 and Table 2.

The calculated *g*-values and associated anisotropies for both cation and neutral radicals are summarized in Table 1. Comparing the predicted Δg of the cation and neutral radical forms, at 406.4 GHz, L-Trp, 5-F-Trp, and 7-OH-Trp cation

Table 2. Calculated Energies (kcal mol^{-1}) of Different Forms of Neutral Indole Radicals As Compared to 1

	X	Y	4CH	4NH	6CH	6NH
unsubs	H	H	36.8310	20.4730	37.4073	21.2050
7-OH	H	OH	39.9200	23.4033	40.8399	24.1682
5-OH	OH	H	37.5223	23.1598	38.9827	23.6731
5-MeOx	OMe	H	38.8657	24.3535	38.1734	23.2923
5-F	F	H	37.9905	22.1130	39.2172	22.6526

DOI: 10.1021/acs.jpca.7b12434
J. Phys. Chem. A 2018, 122, 3170−3176

radicals are all expected to give rise to spectra with axial splitting, whereas neutral radicals should show fully resolved, rhombic patterns. Therefore, because the experimentally observed spectra are not fully resolved, they are expected to arise from their respective cationic radicals. For both 5-OH-Trp and 5-MeOx-Trp, the calculated Δg for the cationic forms are closer to the experimental data than the neutral forms; however, the difference is less significant than that of the other tryptophan-based compounds. As such, *g*-anisotropy alone is insufficient to determine the protonation state of 5-OH-Trp and 5-MeOx-Trp radicals. A summary of tryptophan-based radicals characterized by HFEPR and our predicted neutral radicals can be found in Figure 3.

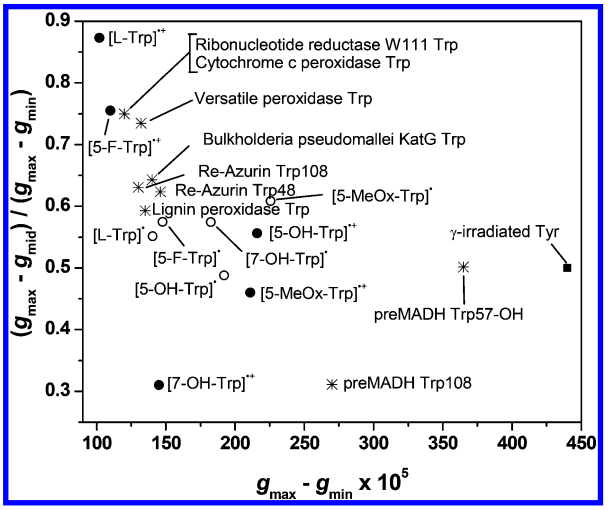

Figure 3. Plot of *g*-value anisotropy versus rhombicity of various tryptophan radical species. Tryptophan-based radicals measured in protein are represented by stars, cation radicals measured in this work are closed circles, and neutral radicals (as calculated in this study) are open circles. The *y*-axis shows rhombicity, where 1.0 and 0.0 would both be completely axial, and the *x*-axis shows *g*-value anisotropy, with 0 representing a purely isotropic signal.

To gain insight into the origin of Δg, spin populations were considered for each of the potential radical species. Mulliken spin populations are schematically shown by the size of circles in Figure 4A, and summarized in Table 3. Spin density distributions have also been previously measured for L-Trp and related compounds in solution by rapid mixing with Ce(IV) as an oxidant, and those distributions are in qualitative agreement with our cationic L-Trp radical.[38] L-Trp and 5-F-Trp have similar spin distributions with the largest spin population on C3 in both cation and neutral radical forms. One significant difference between neutral and cationic L-Trp radicals is that only the cationic species show radical spin density on C2, the position of the cross-link in TTQ. Similarly, 7-OH-Trp shows significant spin density on its TTQ cross-linked carbon, C4, which is diminished upon deprotonation (Figure 4B). Of the compounds studied, only 5-OH-Trp and 5-MeOx-Trp show any spin density at the C5 position and the corresponding substituted oxygen, leading to their rhombic spectra.

CONCLUSION

We have shown for the first time, through the novel use of a photocatalyst system that can generate organic radicals at cryogenic temperatures in a frozen glass without the need for ionizing radiation, HFEPR spectra of L-Trp and 7-OH-Trp in free solution. Producing radicals in this way prevents generation of confounding signals from solvated electrons or other unwanted free radicals. Cationic radical spectra were collected for species relevant to the formation of TTQ in MADH, and the experimental *g*-anisotropies were interpreted in terms of spin populations. The experimental HFEPR spectral patterns are sensitive to the location of oxygen substitution. The cationic radicals have low pK_a values and thus would be expected to decay to neutral radicals spontaneously. The neutral radical forms are predicted to give rhombic spectra, mainly due to delocalization on N1 and C3 positions, even in the absence of oxygen substitution. As related to TTQ biosynthesis, the C2 of an L-Trp residue, and the C4 of a 7-OH-Trp residue form a new covalent bond. This study shows that the radical recombination that forms the TTQ cross-link may be more likely when the respective Trp-based radicals are in their protonated states

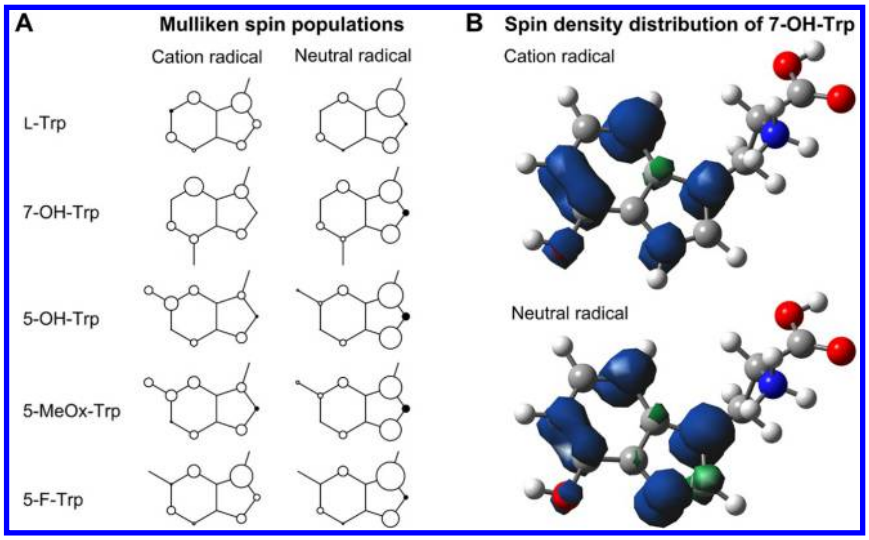

Figure 4. (A) Mulliken spin populations (p-orbital π-component) for the radical forms of tryptophan derivatives. The open and solid circles symbolize positive and negative spin densities, respectively. The size of the circles represents the magnitude of the density. (B) Three-dimensional representation of the spin density distribution of cationic and neutral 7-OH-Trp radicals.

DOI: 10.1021/acs.jpca.7b12434
J. Phys. Chem. A 2018, 122, 3170−3176

Table 3. Mulliken Spin Populations (pπ/p-Component) for Both Radicals of Tryptophan Derivatives

Cation Radical										
	unsubs		7-OH		5-OH		5-MeOx		5-F	
1N	0.12	0.13	0.16	0.18	0.15	0.18	0.16	0.19	0.14	0.16
2C	0.12	0.11	−0.03	−0.06	−0.03	−0.05	−0.06	−0.08	0.09	0.08
3C	0.31	0.40	0.21	0.27	0.10	0.11	0.12	0.15	0.36	0.45
4C	0.22	0.27	0.32	0.40	0.15	0.17	0.19	0.23	0.22	0.28
5C	−0.07	−0.11	−0.02	−0.05	0.23	0.26	0.18	0.20	−0.05	−0.08
6C	0.18	0.22	0.15	0.17	−0.02	−0.04	−0.03	−0.06	0.14	0.18
7C	0.05	0.05	0.15	0.17	0.10	0.11	0.12	0.15	0.04	0.04
O or F			0.09	0.09	0.14	0.14	0.15	0.16	0.00	0.00
Neutral Radical										
	unsubs		7-OH		5-OH		5-MeOx		5-F	
1N	0.25	0.26	0.29	0.31	0.36	0.38	0.34	0.37	0.27	0.29
2C	−0.05	−0.10	−0.10	−0.15	−0.12	−0.17	−0.12	−0.17	−0.08	−0.13
3C	0.45	0.57	0.35	0.44	0.33	0.40	0.32	0.40	0.46	0.59
4C	0.17	0.22	0.21	0.27	0.15	0.17	0.16	0.19	0.17	0.21
5C	−0.04	−0.07	0.01	−0.01	0.12	0.13	0.11	0.12	−0.02	−0.04
6C	0.14	0.17	0.12	0.14	−0.05	−0.07	−0.05	−0.07	0.10	0.13
7C	0.03	0.02	0.10	0.10	0.14	0.18	0.15	0.19	0.03	0.03
O or F			0.04	0.04	0.05	0.05	0.06	0.07	0.00	0.00

because the carbon atoms of L-Trp and 7-OH-Trp that form the cross-link have more radical character in their respective protonated states. This finding provides new physical insight about the unusual 7-OH-Trp radical and opens a new possibility for the cross-linking reaction, as it was previously thought that the cation radicals initially generated by MauG would have to spontaneously deprotonate before cross-link formation.[22]

■ ASSOCIATED CONTENT

Supporting Information

The Supporting Information is available free of charge on the ACS Publications website at DOI: 10.1021/acs.jpca.7b12434.

Table S1 of the calculation of the *g*-values of tryptophan compounds without COSMO and ten additional figures (i.e., Figures S1−S10) of full HFEPR spectra and X-band EPR data (PDF)

■ AUTHOR INFORMATION

Corresponding Author

*Address correspondence to Aimin Liu Department of Chemistry University of Texas at San Antonio One UTSA Circle San Antonio, TX 78249, USA Tel: +1-210-458-7062 E-mail: Feradical@utsa.edu.

ORCID

Aimin Liu: 0000-0002-4182-8176

Author Contributions

¶These authors contributed equally to this work.

Notes

The authors declare no competing financial interest.

■ ACKNOWLEDGMENTS

We thank Dr. A. Ozarowski for his software package DOUBLET. This work was supported in whole or part by the National Institutes of Health (NIH) Grant GM108988, the National Science Foundation (NSF) grant CHE-1623856, and the Lutcher Brown Distinguished Chair Endowment fund (to A.L.). We are indebted to The Texas Advanced Computing Center (TACC) for accessing computational resources. Part of this work was conducted at the National High Magnetic Field Laboratory is funded by the NSF through a Cooperative Agreement DMR 1157490, the State of Florida, and the U.S. Department of Energy.

■ REFERENCES

(1) Popova, N. K. From genes to agressive behavior: the role of serotonergic system. *BioEssays* **2006**, *28*, 495−503.

(2) Vanecek, J. Cellular mechanisms of melatonin action. *Physiol. Rev.* **1998**, *78*, 687−721.

(3) Stone, T. W.; Darlington, L. G. Endogenous kynurenines as targets for drug discovery and development. *Nat. Rev. Drug Discovery* **2002**, *1*, 609−620.

(4) Kurnasov, O.; Goral, V.; Colabroy, K.; Gerdes, S.; Anantha, S.; Osterman, A.; Begley, T. P. NAD biosynthesis: identification of the tryptophan to quinolinate pathway in bacteria. *Chem. Biol.* **2003**, *10*, 1195−1204.

(5) Stone, T. W.; Mackay, G. M.; Forrest, C. M.; Clark, C. J.; Darlington, L. G. Tryptophan metabolites and brain disorders. *Clin. Chem. Lab. Med.* **2003**, *41*, 852−859.

(6) Gholson, R. K.; Rao, D. R.; Henderson, L. M.; Hill, R. J.; Koeppe, R. E. The metabolism of DL-tryptophan-7α-C^{14} by the rat. *J. Biol. Chem.* **1957**, *230*, 197−184.

(7) Samanta, U.; Pal, D.; Chakrabarti, P. Environment of tryptophan side chains in proteins. *Proteins: Struct., Funct., Genet.* **2000**, *38*, 288−300.

(8) Nelson, N.; Yocum, C. F. Structure and function of photosystems I and II. *Annu. Rev. Plant Biol.* **2006**, *57*, 521−565.

(9) Byrdin, M.; Eker, A. P. M.; Vos, M. H.; Brettel, K. Dissection of the triple tryptophan electron transfer chain in *Escherichia coli* DNA photolyase: Trp382 is the primary donor in photoactivation. *Proc. Natl. Acad. Sci. U. S. A.* **2003**, *100*, 8676−8681.

(10) McIntire, W. S.; Wemmer, D. E.; Chistoserdov, A.; Lidstrom, M. E. A new cofactor in a prokaryotic enzyme: tryptophan tryptophylquinone as the redox prosthetic group in methylamine dehydrogenase. *Science* **1991**, *252*, 817−824.

(11) Datta, S.; Mori, Y.; Takagi, K.; Kawaguchi, K.; Chen, Z.-W.; Okajima, T.; Kuroda, S.; Ikeda, T.; Kano, K.; Tanizawa, K.; Mathews, F. S. Structure of a quinohemoprotein amine dehydrogenase with an uncommon redox cofactor and highly unusual crosslinking. *Proc. Natl. Acad. Sci. U. S. A.* **2001**, *98*, 14268−14273.

DOI: 10.1021/acs.jpca.7b12434
J. Phys. Chem. A 2018, 122, 3170−3176

(12) Ivancich, A.; Dorlet, P.; Goodin, D. B.; Un, S. Multifrequency high-field EPR study of the tryptophanyl and tyrosyl radical intermediates in wild-type and the W191G mutant of cytochrome c peroxidase. *J. Am. Chem. Soc.* **2001**, *123*, 5050−5058.
(13) Colin, J.; Wiseman, B.; Switala, J.; Loewen, P. C.; Ivancich, A. Distinct role of specific tryptophans in facilitating electron transfer or as [Fe(IV)═O Trp(*)] intermediates in the peroxidase reaction of *Bulkholderia pseudomallei* catalase-peroxidase: a multifrequency EPR spectroscopy investigation. *J. Am. Chem. Soc.* **2009**, *131*, 8557−8563.
(14) Smith, A. T.; Doyle, W. A.; Dorlet, P.; Ivancich, A. Spectroscopic evidence for an engineered, catalytically active Trp radical that creates the unique reactivity of lignin peroxidase. *Proc. Natl. Acad. Sci. U. S. A.* **2009**, *106*, 16084−16089.
(15) Pogni, R.; Baratto, M. C.; Teutloff, C.; Giansanti, S.; Ruiz-Duenas, F. J.; Choinowski, T.; Piontek, K.; Martinez, A. T.; Lendzian, F.; Basosi, R. A tryptophan neutral radical in the oxidized state of versatile peroxidase from *Pleurotus eryngii*: a combined multifrequency EPR and density functional theory study. *J. Biol. Chem.* **2006**, *281*, 9517−9526.
(16) Stoll, S.; Shafaat, H. S.; Krzystek, J.; Ozarowski, A.; Tauber, M. J.; Kim, J. E.; Britt, R. D. Hydrogen bonding of tryptophan radicals revealed by EPR at 700 GHz. *J. Am. Chem. Soc.* **2011**, *133*, 18098−18101.
(17) Potsch, S.; Lendzian, F.; Ingemarson, R.; Hornberg, A.; Thelander, L.; Lubitz, W.; Lassmann, G.; Gräslund, A. The iron-oxygen reconstitution reaction in protein R2-Tyr-177 mutants of mouse ribonucleotide reductase. EPR and electron nuclear double resonance studies on a new transient tryptophan radical. *J. Biol. Chem.* **1999**, *274*, 17696−17704.
(18) Bleifuss, G.; Kolberg, M.; Potsch, S.; Hofbauer, W.; Bittl, R.; Lubitz, W.; Gräslund, A.; Lassmann, G.; Lendzian, F. Tryptophan and tyrosine radicals in ribonucleotide reductase: a comparative high-field EPR study at 94 GHz. *Biochemistry* **2001**, *40*, 15362−15368.
(19) Olshansky, L.; Greene, B. L.; Finkbeiner, C.; Stubbe, J.; Nocera, D. G. Photochemical generation of a tryptophan radical within the subunit interface of ribonucleotide reductase. *Biochemistry* **2016**, *55*, 3234−3240.
(20) Wang, Y.; Graichen, M. E.; Liu, A.; Pearson, A. R.; Wilmot, C. M.; Davidson, V. L. MauG, a novel diheme protein required for tryptophan tryptophylquinone biogenesis. *Biochemistry* **2003**, *42*, 7318−7325.
(21) Li, X.; Fu, R.; Lee, S.; Krebs, C.; Davidson, V. L.; Liu, A. A catalytic di-heme *bis*-Fe(IV) intermediate, alternative to an Fe(IV)═O porphyrin radical. *Proc. Natl. Acad. Sci. U. S. A.* **2008**, *105*, 8597−8600.
(22) Yukl, E. T.; Liu, F.; Krzystek, J.; Shin, S.; Jensen, L. M. R.; Davidson, V. L.; Wilmot, C. M.; Liu, A. Diradical intermediate within the context of tryptophan tryptophylquinone biosynthesis. *Proc. Natl. Acad. Sci. U. S. A.* **2013**, *110*, 4569−4573.
(23) Svistunenko, D. A.; Wilson, M. T.; Cooper, C. E. Tryptophan or tyrosine? On the nature of the amino acid radical formed following hydrogen peroxide treatment of cytochrome *c* oxidase. *Biochim. Biophys. Acta, Bioenerg.* **2004**, *1655*, 372−380.
(24) Abe, M. Diradicals. *Chem. Rev.* **2013**, *113*, 7011−7088.
(25) Al-Kazwini, A. T.; O'Neill, P.; Adams, G. E.; Cundall, R. B.; Junino, A.; Maignan, J. Characterisation of the intermediates produced upon one-electron oxidation of 4-, 5-, 6- and 7-hydroxyindoles by the azide radical. *J. Chem. Soc., Perkin Trans. 2* **1992**, 657−661.
(26) Pizano, A. A.; Lutterman, D. A.; Holder, P. G.; Teets, T. S.; Stubbe, J.; Nocera, D. G. Photo-ribonucleotide reductase β2 by selective cysteine labeling with a radical phototrigger. *Proc. Natl. Acad. Sci. U. S. A.* **2012**, *109*, 39−43.
(27) Hassan, A. K.; Pardi, L. A.; Krzystek, J.; Sienkiewicz, A.; Goy, P.; Rohrer, M.; Brunel, L.-C. Ultrawide band multifrequency high-field EMR technique: A methodology for increasing spectroscopic information. *J. Magn. Reson.* **2000**, *142*, 300−312.
(28) Stoll, S.; Ozarowski, A.; Britt, R. D.; Angerhofer, A. Atomic hydrogen as high-precision field standard for high-field EPR. *J. Magn. Reson.* **2010**, *207*, 158−163.
(29) Zvyagin, S. A.; Krzystek, J.; van Loosdrecht, P. H. M.; Dhalenne, G.; Revcolevschi, A. High-field ESR study of the dimerized-incommensurate phase transition in the spin-Peierls compound $CuGeO_3$. *Phys. B* **2004**, *346−347*, 1−5.
(30) Ozarowski, A.; Lee, H. M.; Balch, A. L. Crystal environments probed by EPR spectroscopy. Variations in the EPR spectra of Co(II)(octaethylporphyrin) doped in crystalline diamagnetic hosts and a reassessment of the electronic structure of four-coordinate cobalt(II). *J. Am. Chem. Soc.* **2003**, *125*, 12606−12614.
(31) Neese, F. The ORCA program system. *Comput. Mol. Sci.* **2012**, *2*, 73−78.
(32) Neese, F.; Wennmohs, F.; Hansen, A.; Becker, U. Efficient, approximate and parallel Hartree−Fock and hybrid DFT calculations. A 'chain-of-spheres' algorithm for the Hartree−Fock exchange. *Chem. Phys.* **2009**, *356*, 98−109.
(33) Petrenko, T.; Kossmann, S.; Neese, F. Efficient time-dependent density functional theory approximations for hybrid density functionals: analytical gradients and parallelization. *J. Chem. Phys.* **2011**, *134*, 054116.
(34) Klamt, A.; Schuurmann, G. COSMO: a new approach to dielectric screening in solvents with explicit expressions for the screening energy and its gradient. *J. Chem. Soc., Perkin Trans. 2* **1993**, 799−805.
(35) Sinnecker, S.; Rajendran, A.; Klamt, A.; et al. Calculation of solvent shifts on electronic g-tensors with the conductor-like screening model (COSMO) and its self-consistent generalizatoin to real solvents (COSMO-RS). *J. Phys. Chem. A* **2006**, *110*, 2235−2245.
(36) Drago, R. S. *Physical Methods in Chemistry*, 2nd ed.; W. B. Saunders Co.: Philadelphia, 1992.
(37) Liu, A.; Barra, A.-L.; Rubin, H.; Lu, G.; Gräslund, A. Heterogeneity of the local electrostatic environment of the tyrosyl radical in *Mycobacterium tuberculosis* ribonucleotide reductase observed by high-field EPR spectroscopy. *J. Am. Chem. Soc.* **2000**, *122*, 1974−1978.
(38) Connor, H. D.; Sturgeon, B. E.; Mottley, C.; Sipe, H. J.; Mason, R. P. L-Tryptophan radical cation electron spin resonance studies: connecting solution-derived hyperfine coupling constants with protein spectral interpretations. *J. Am. Chem. Soc.* **2008**, *130*, 6381−6387.

DOI: 10.1021/acs.jpca.7b12434
J. Phys. Chem. A 2018, 122, 3170−3176

Supplemental information for

High-Frequency/High-Field EPR and Theoretical Studies of Tryptophan-Based Radicals

Ian Davis[†‡], Teruaki Koto[†], James R. Terrell[‡], Alexander Kozhanov[§], J. Krzystek[Δ], and Aimin Liu[†*]

[†]Department of Chemistry, University of Texas, San Antonio, Texas 78249, United States;

[‡]Department of Chemistry, Georgia State University, Atlanta, Georgia 30303, United States;

[§]Department of Physics, Georgia State University, Atlanta, Georgia 30303, United States;

[Δ]National High Magnetic Field Laboratory, Florida State University, Tallahassee, Florida 32310, United States

This supplemental material contains the following:

Table S1. Calculation of the *g*-values of tryptophan compounds without COSMO.

Figure S1. Full HFEPR spectrum of L-tryptophan and field standard (average of 16 scans) at 406.4 GHz, 0.3 mT modulation amplitude, 4.5 K (black trace) and corresponding simulated spectrum (blue trace).

Figure S2. Full HFEPR spectrum of D-tryptophan and field standard (average of 10 scans) at 406.4 GHz, 0.3 mT modulation amplitude, 4.5 K (black trace) and corresponding simulated spectrum (blue trace).

Figure S3. Full HFEPR spectrum of 5-fluorotryptophan and field standard (average of 20 scans) at 406.4 GHz, 0.3 mT modulation amplitude, 4.5 K (black trace) and corresponding simulated spectrum (blue trace).

Figure S4. Full HFEPR spectrum of 5-methoxytryptophan and field standard (average of 30 scans) at 406.4 GHz, 0.3 mT modulation amplitude, 4.5 K (black trace) and corresponding simulated spectrum (blue trace).

Figure S5. Full HFEPR spectrum of 5-hydroxytryptophan and field standard (average of 25 scans) at 406.4 GHz, 0.3 mT modulation amplitude, 4.5 K (black trace) and corresponding simulated spectrum (blue trace).

Figure S6. Full HFEPR spectrum of 7-hydroxytryptophan and field standard (average of 16 scans) at 406.4 GHz, 0.3 mT modulation amplitude, 4.5 K (black trace) and corresponding simulated spectrum (blue trace).

Figure S7. X-band EPR spectrum of L-tryptophan radical. Radical was generated as described in the materials and methods. Instrument parameters: 9.6 GHz, 100 kHz modulation frequency, 0.01 mT modulation amplitude, 77 K.

Figure S8. X-band EPR spectrum of 5-hydroxytryptophan radical. Radical was generated as described in the materials and methods. Instrument parameters: 9.6 GHz, 100 kHz modulation frequency, 0.01 mT modulation amplitude, 77 K.

Figure S9. X-band EPR spectrum of 5-methoxytryptophan radical. Radical was generated as described in the materials and methods. Instrument parameters: 9.6 GHz, 100 kHz modulation frequency, 0.01 mT modulation amplitude, 77 K.

Figure S10. X-band EPR spectrum of 7-hydroxytryptophan radical. Radical was generated as described in the materials and methods. Instrument parameters: 9.6 GHz, 100 kHz modulation frequency, 0.01 mT modulation amplitude, 77 K.

Table S1. Calculation of the *g*-values of tryptophan compounds without COSMO.

		g_{min}	g_{mid}	g_{max}	Span[a]	Span / L-Trp	Skew[b]
L-Trp	experiment	2.00227	2.00240	2.00329	102	-	0.873
	cation	2.00229	2.00250	2.00332	103	-	0.792
	neutral	2.00227	2.00298	2.00427	200	-	0.646
7-OH-Trp	experiment	2.00213	2.00313	2.00358	145	1.422	0.310
	cation	2.00226	2.00315	2.00390	164	1.594	0.459
	neutral	2.00226	2.00298	2.00477	251	1.256	0.713
5-OH-Trp	experiment	2.00223	2.00319	2.00439	216	2.118	0.556
	cation	2.00224	2.00320	2.00443	219	2.126	0.561
	neutral	2.00224	2.00329	2.00466	242	1.210	0.569
5-MeOx-Trp	experiment	2.00205	2.00319	2.00416	211	2.069	0.460
	cation	2.00222	2.00356	2.00472	250	2.432	0.465
	neutral	2.00223	2.00306	2.00504	281	1.404	0.705
5-F-Trp	experiment	2.00217	2.00244	2.00327	110	1.078	0.755
	cation	2.00221	2.00369	2.00434	214	2.077	0.306
	neutral	2.00224	2.00321	2.00494	270	1.353	0.639

[a.] Span is Δg, the difference between g_{min} and $g_{max} \times 10^5$.

[b.] Skew is g_{max}-g_{mid}/g_{max}-g_{min}

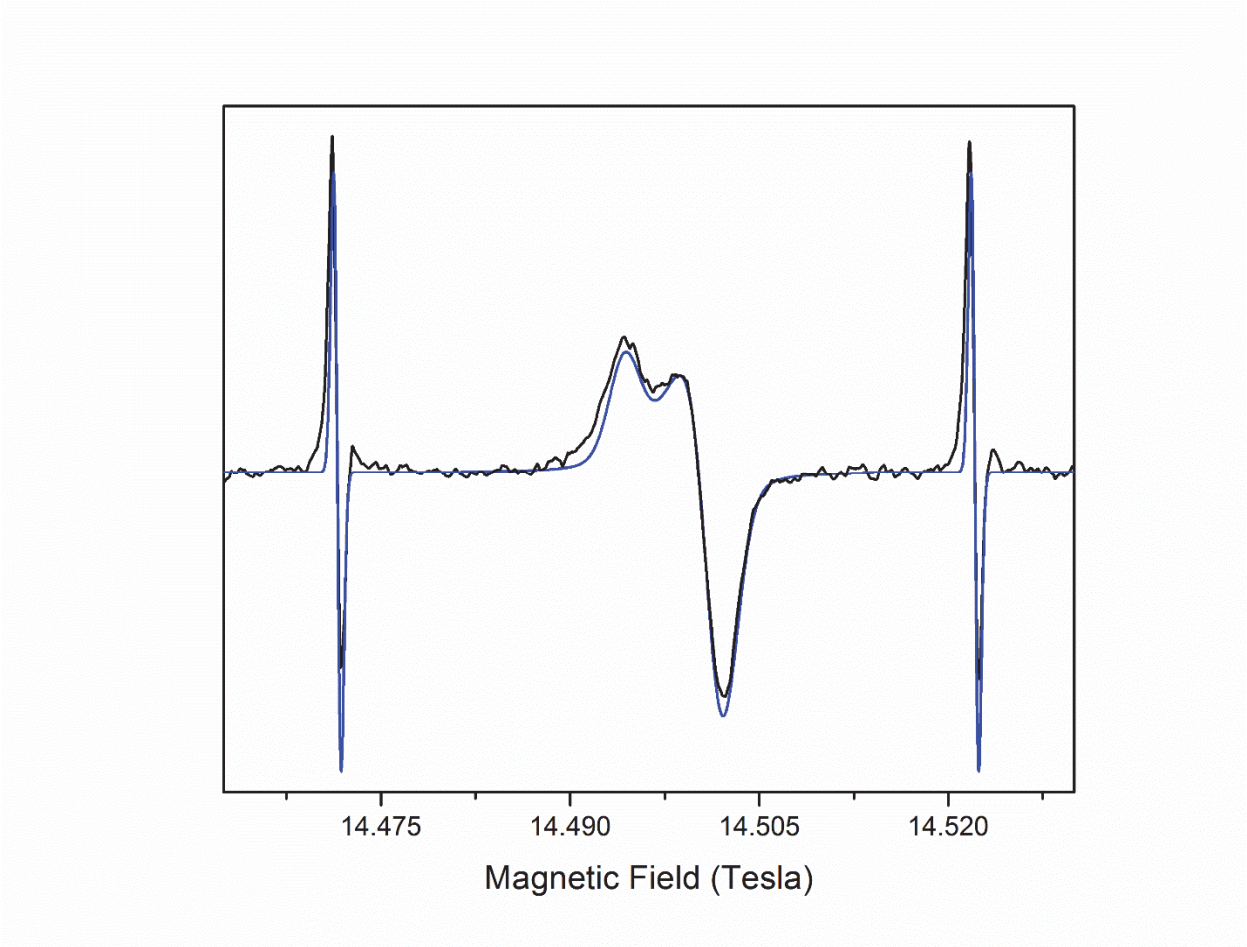

Figure S1. Full HFEPR spectrum of L-tryptophan and field standard (average of 16 scans) at 406.4 GHz, 0.3 mT modulation amplitude, 4.5 K (black trace) and corresponding simulated spectrum (blue trace).

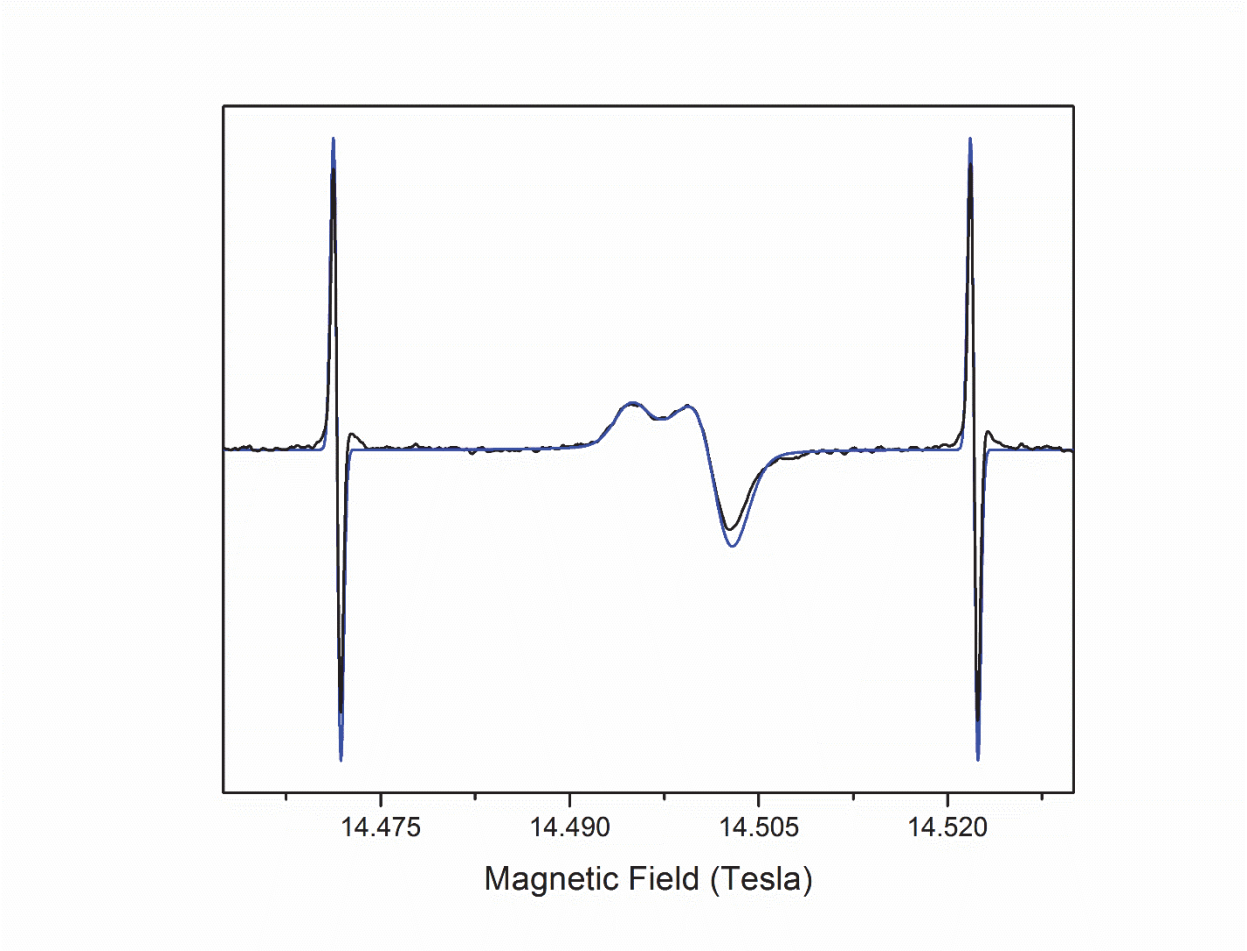

Figure S2. Full HFEPR spectrum of D-tryptophan and field standard (average of 10 scans) at 406.4 GHz, 0.3 mT modulation amplitude, 4.5 K (black trace) and corresponding simulated spectrum (blue trace).

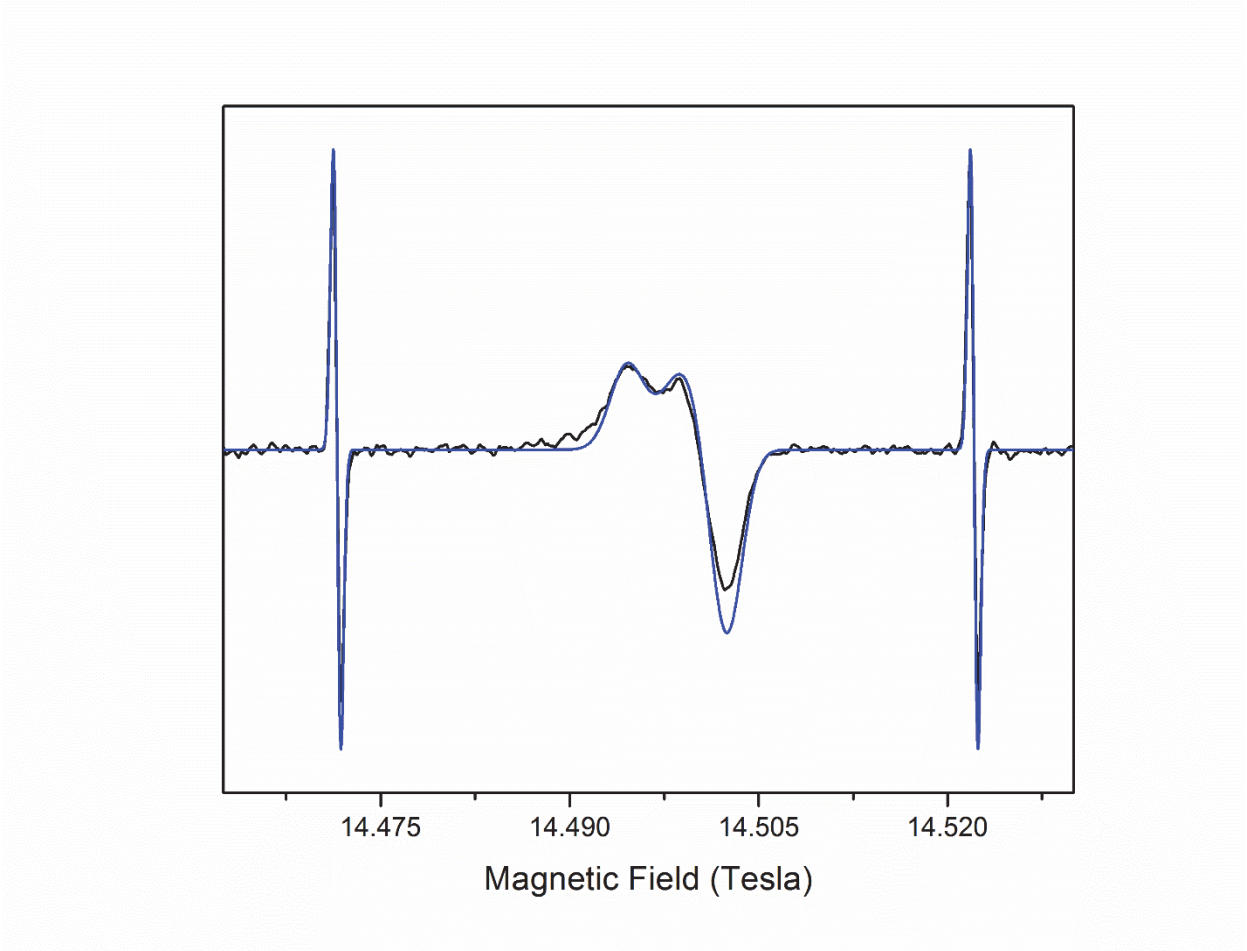

Figure S3. Full HFEPR spectrum of 5-fluorotryptophan and field standard (average of 20 scans) at 406.4 GHz, 0.3 mT modulation amplitude, 4.5 K (black trace) and corresponding simulated spectrum (blue trace).

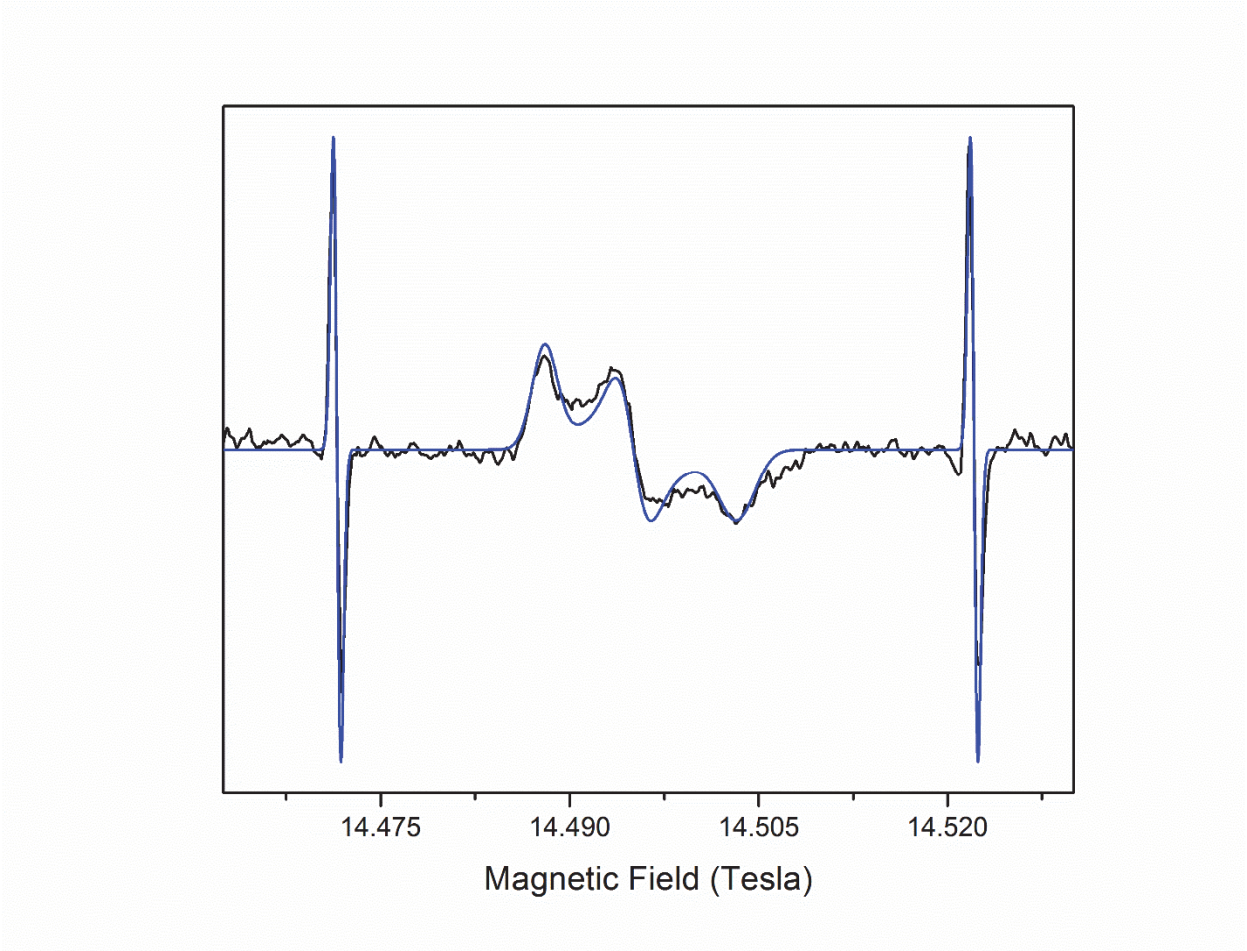

Figure S4. Full HFEPR spectrum of 5-methoxytryptophan and field standard (average of 30 scans) at 406.4 GHz, 0.3 mT modulation amplitude, 4.5 K (black trace) and corresponding simulated spectrum (blue trace).

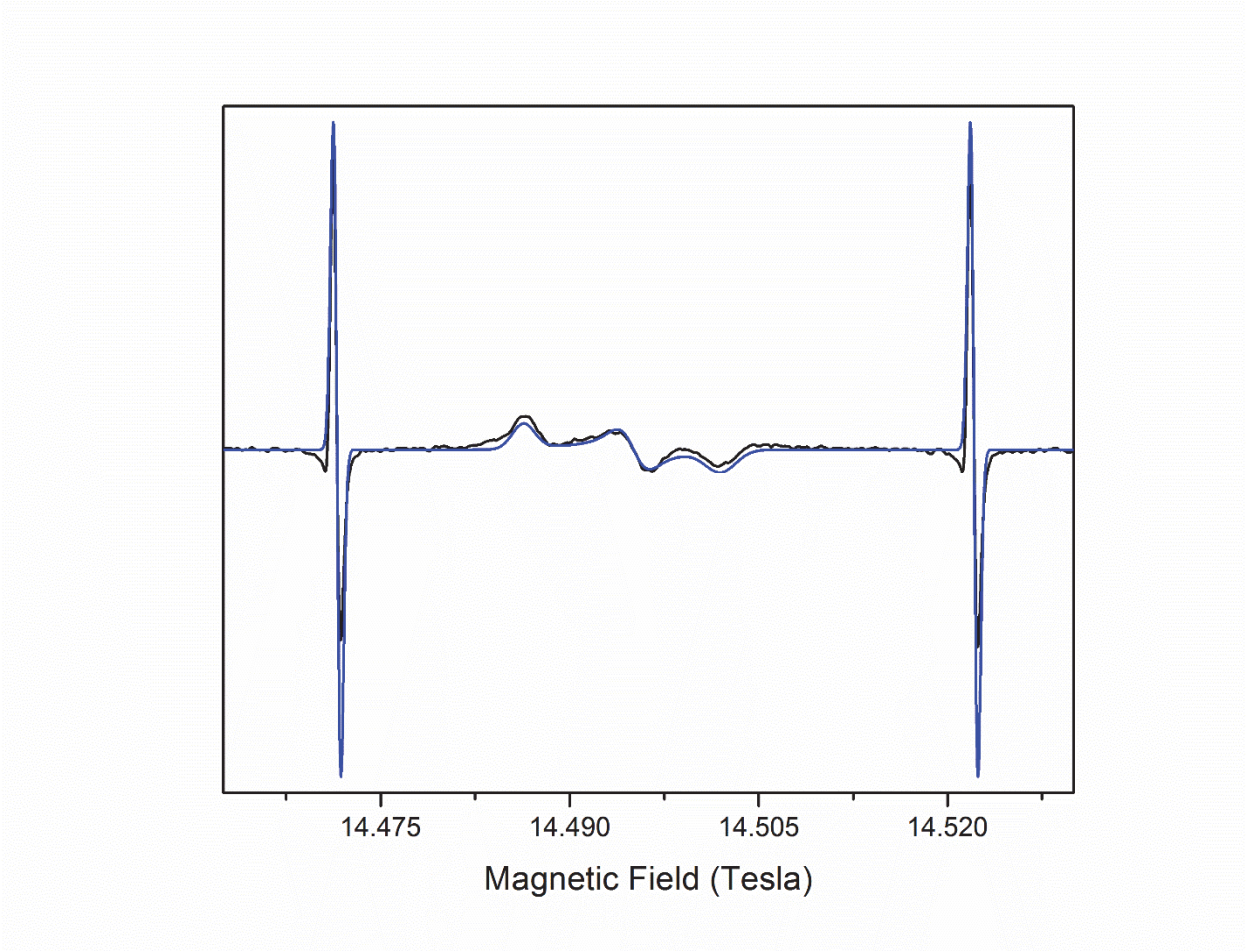

Figure S5. Full HFEPR spectrum of 5-hydroxytryptophan and field standard (average of 25 scans) at 406.4 GHz, 0.3 mT modulation amplitude, 4.5 K (black trace) and corresponding simulated spectrum (blue trace).

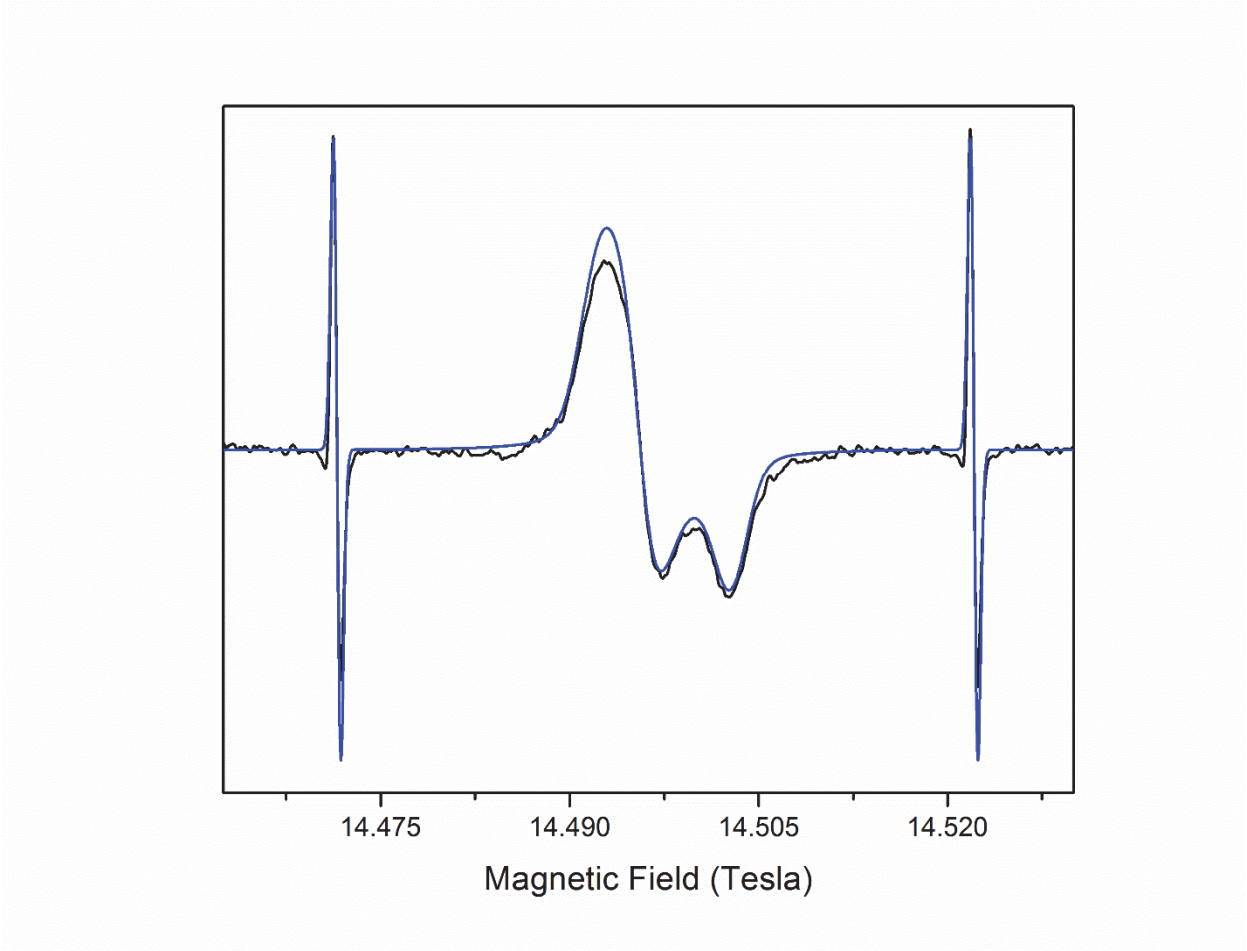

Figure S6. Full HFEPR spectrum of 7-hydroxytryptophan and field standard (average of 16 scans) at 406.4 GHz, 0.3 mT modulation amplitude, 4.5 K (black trace) and corresponding simulated spectrum (blue trace).

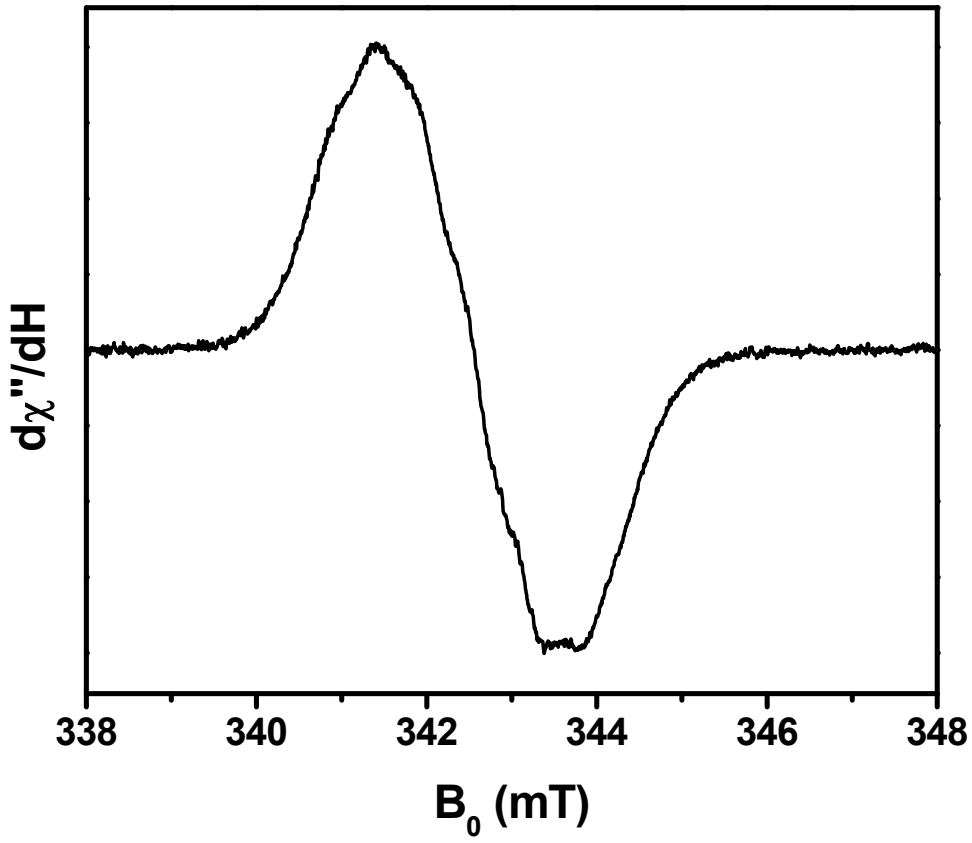

Figure S7. X-band EPR spectrum of L-tryptophan radical. Radical was generated as described in the materials and methods. Instrument parameters: 9.6 GHz, 100 kHz modulation frequency, 0.01 mT modulation amplitude, 77 K.

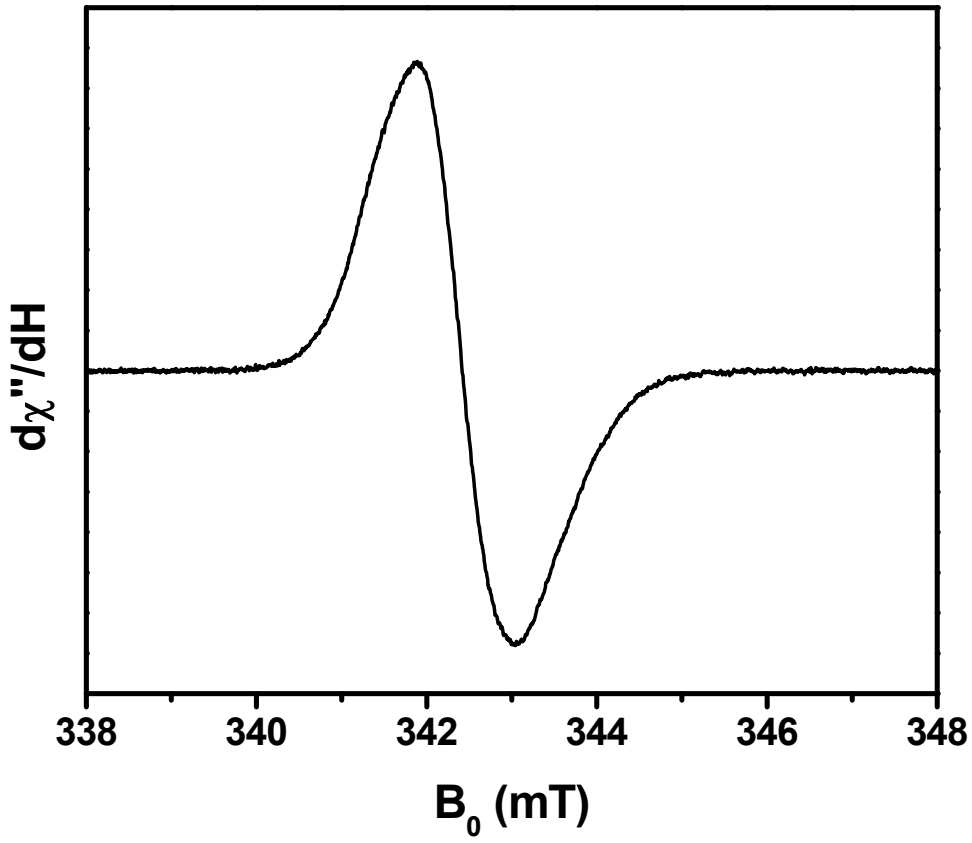

Figure S8. X-band EPR spectrum of 5-hydroxytryptophan radical. Radical was generated as described in the materials and methods. Instrument parameters: 9.6 GHz, 100 kHz modulation frequency, 0.01 mT modulation amplitude, 77 K.

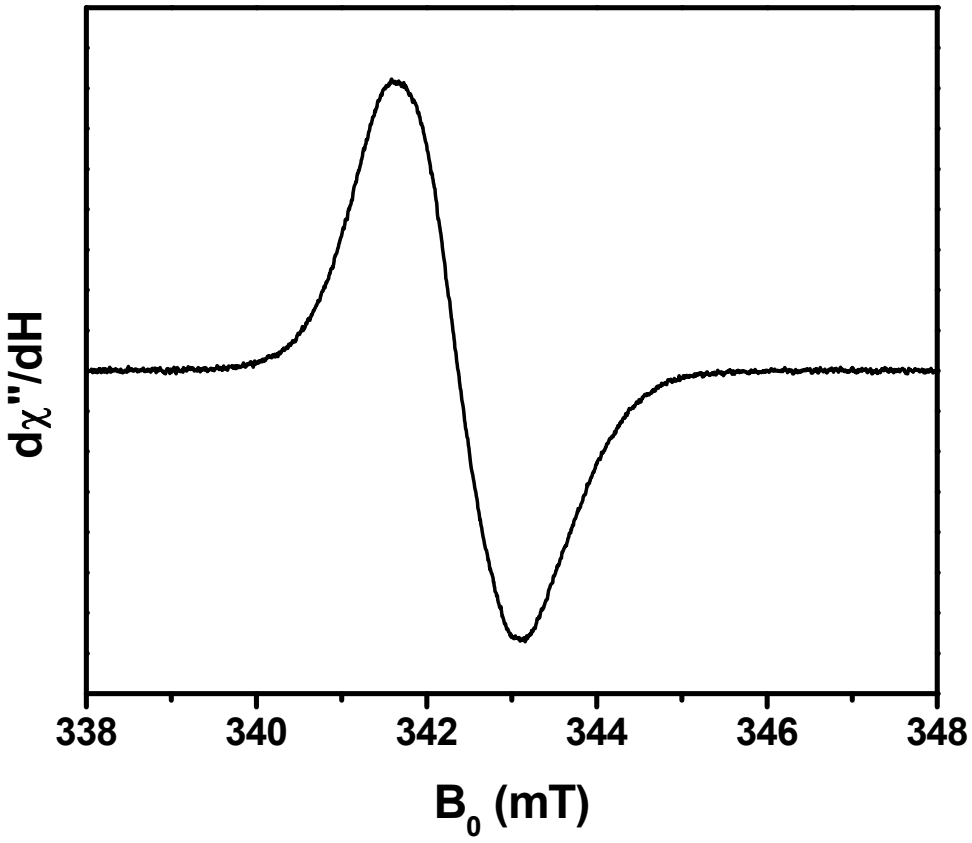

Figure S9. X-band EPR spectrum of 5-methoxytryptophan radical. Radical was generated as described in the materials and methods. Instrument parameters: 9.6 GHz, 100 kHz modulation frequency, 0.01 mT modulation amplitude, 77 K.

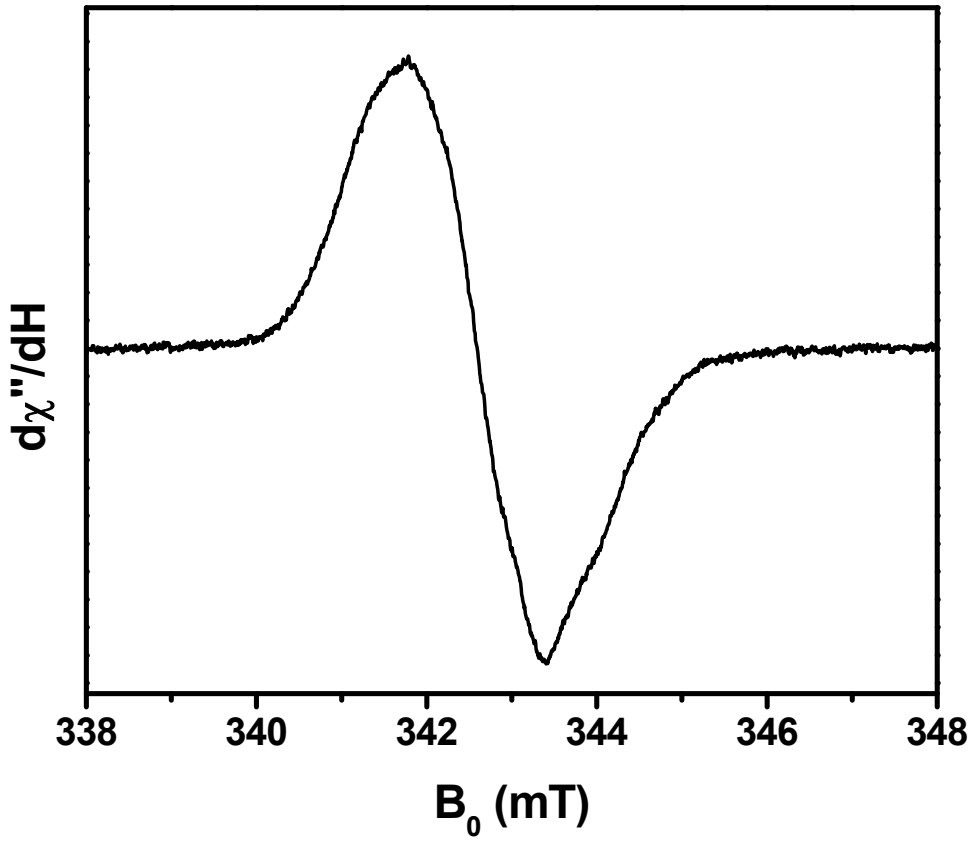

Figure S10. X-band EPR spectrum of 7-hydroxytryptophan radical. Radical was generated as described in the materials and methods. Instrument parameters: 9.6 GHz, 100 kHz modulation frequency, 0.01 mT modulation amplitude, 77 K.